AIAA JOURNAL
Vol. 50, No. 6, June 2012

Bag Breakup of Turbulent Liquid Jets in Crossflows

Xiong-hui Wang,* Yong Huang,† Shao-lin Wang,‡ and Zhi-lin Liu‡
Beihang University, 100191 Beijing, People's Republic of China

DOI: 10.2514/1.J051451

An experiment was conducted to investigate the bag breakup process of round liquid jets in crossflows. A high-speed camera was used to observe the formation and breakup of bags in a water jet from a 1.0 mm diameter nozzle with a Weber number in the range of 11 ∼ 36 and the liquid-to-air momentum ratio from 11 to 95. An analysis of the force balance on bags was conducted and a criterion for bag formation is obtained. The diameter of the bag ring tube was predicted according to a reduced-order model, and the predicted results agree qualitatively well with the experiments. Present results indicate that the normalized basal ring diameter, ring tube diameter, and the bag onset time are all constants, while the onset length of bags normalized by the initial jet diameter varies with the liquid-to-air momentum ratio and jet Reynolds number. The bag breakup length decreases linearly with the increase of the Weber number, and is independent of the liquid jet velocity. The streamwise distance of the breakup location from the nozzle exit is a constant, while the cross-stream distance increases with the liquid-to-air momentum ratio.

Nomenclature

d_r	=	basal ring diameter
d_0	=	initial jet diameter
d_t	=	bag ring tube diameter
C_D	=	drag coefficient
C_1	=	empirical constant
C_2	=	empirical constant
C_3	=	empirical constant
l_{onset}	=	bag onset length
q	=	liquid–air momentum flux ratio, $q = \rho_j v_j^2/\rho_G u_G^2$
Re_j	=	jet Reynolds number, $Re_j = \rho_j v_j d_0/\mu_j$
t_{onset}	=	bag onset time
t^*	=	aerodynamic characteristic time, $t^* = d_0(\rho_j/\rho_G)^{1/2}/u_G$
We_G	=	air Weber number, $We_G = \rho_G u_G^2 d_0/\sigma$
x_{onset}	=	X coordinate of bag onset point
y_{onset}	=	Y coordinate of bag onset point
x_b	=	X coordinate of jet breakup point
y_b	=	Y coordinate of jet breakup point
σ	=	liquid surface tension coefficient

I. Introduction

THE breakup and atomization of liquid jets in gaseous crossflows has widespread applications in propulsion systems such as gas turbine combustors, turbojet afterburners, and ramjet and scramjet combustors [1]. In recent times, the concept of lean, premixed, prevaporized (LPP) combustion has generated significant interest in aerospace propulsion applications because of its potential to reduce the emission of oxides of nitrogen NO_x. The plain fuel jet in crossflows configuration is a potential candidate for LPP combustors due to its rapid atomization and controllable fuel placement [2]. Combustion efficiency, lean blow out limits, and combustion dynamics are also dependent upon the quality of liquid fuel atomization.

Earlier studies revealed the breakup process of liquid jets injected into crossflows. The dynamic pressure of the crossflow causes the jet to flatten and bend in the direction of the crossflow [3]. After bending, the jet soon undergoes breakup to form ligaments and droplets [4]. Empirical correlations have been developed to describe the column breakup location [4,5] and droplets' diameters [5]. Wu et al. [4] found that the x distances to the column fracture point were a constant, while the transverse distances to the fracture point increased were correlated with liquid–air momentum flux ratio q alone. Sallam et al. [5] obtained the same conclusion from their experiment. The jet trajectory and penetration have also received considerable attention. In all the previous studies [6–9], the penetration of the jet was found to be dependent upon liquid–air momentum flux ratio and the nozzle's diameter. Tambe et al. [6] used logarithmic form to fit a correlation, while Wu et al. [7], Becker and Hassa [8], and Lin et al. [9] employed power-law form to fit the correlation for the jet penetration.

Similarities between the primary and secondary breakup were proposed by Wu et al. [4]. They found that analogy method can be used in primary breakup study. The breakup regime transitions were identified by Wu et al. [4] who constructed a breakup map of liquid jet in crossflow using the crossflow Weber number and liquid–air momentum flux ratio as the map coordinates. Mazallon et al. [10] observed that for low Ohnesorge number, $Oh < 0.1$, the breakup regime transitions are controlled solely by the crossflow Weber number. Then Mazallon et al. [10] reconstructed a breakup regime map in terms of crossflow Weber number and Ohnesorge number as the map coordinates and proposed that the onset of bag breakup initiated at a crossflow Weber number of 5. Another transition to multimode breakup regime happens when the Weber number reaches 60. Later, Sallam et al. [5] modified the boundary for the transition between the bag breakup regime and the multimode breakup regime.

The column breakup location of a liquid jet was studied by Wu et al. [4], who concluded that the streamwise distance to the column breakup location is proportional to the momentum ratio with a power of 0.53 while the cross-stream distance to the column breakup location is a constant of 8.06. Sallam et al. [5] conducted another experiment to investigate the column breakup location and their results were generally in good agreement with that of Wu et al. [4]. Recently Zhu et al. [11,12] demonstrated that both streamwise and cross-stream distances varied with momentum ratio in column breakup regime.

Aalburg et al. [13] observed the onset of ligaments and the formation of droplets. The droplet velocity measurement indicates that the size and velocity of the droplets are unrelated, and that the cross-stream component of the velocity is higher than the streamwise component. Jet velocity along the liquid column was found to be nearly constant. Later, Aalburg et al. [13] studied the deformation of liquid jets by simulation. The bag breakup of a nonturbulent liquid jet in crossflows was studied by Sallam et al. [5], who found the formation and development of the column waves is caused by the

Received 30 June 2011; revision received 28 November 2011; accepted for publication 13 December 2011.

*Graduate Student, National Key Laboratory on Aero-Engines, School of Jet Propulsion.

†Professor, School of Jet Propulsion; yhuang@buaa.edu.cn (Corresponding Author).

‡Graduate Student, School of Jet Propulsion.

Rayleigh–Taylor instability. Three distinctive sizes of droplets, which are node-droplets, ring-droplets, and membrane-droplets, are observed in the bag breakup regime [14]. Ng et al. [15] observed that surface wavelength varied with crossflow Weber number.

The objective of this study is to extend the understanding of the bag breakup process by observing the breakup of a uniform round liquid jet in crossflows. Specifically, this study measures the basal ring diameter, ring tube diameter, bag onset length, bag breakup distance, and the column breakup location. A high-speed camera is used to provide the dynamic information of the primary breakup of the liquid jet. A phenomenological analysis was presented to interpret the measurements.

Table 1 Liquid properties and test conditions

Liquid	Water
Temperature, T/K	$293 \sim 298$
Liquid density, $\rho_L/(\mathrm{kg/m^3})$	996
Gas density, $\rho_G/(\mathrm{kg/m^3})$	1.17
Jet velocity, $v_j/(\mathrm{m \cdot s^{-1}})$	$4.6 \sim 8.1$
Gas velocity, $u_G/(\mathrm{m \cdot s^{-1}})$	$25.2 \sim 37.2$
Liquid viscosity, $\mu_j/(\mu\mathrm{Pa \cdot s})$	854.4
Surface tension, $\sigma/(\mathrm{N/M} \times 10^{-3})$	70.9
Momentum flux ration, q	$11 \sim 95$
Jet Reynolds number, Re_j	$4899 \sim 9798$
Crossflow Weber number, We_G	$11 \sim 36$
Liquid jet Ohnesorge number, Oh	0.0026

II. Experiment Methods

A. Apparatus

Figure 1 shows the schematics of the subsonic wind tunnel and the injection system used in the present study. For a more detailed description, please refer to [16,17]. A pressure injection is used to feed the test liquids stored in a stainless steel cylindrical tank (volume = 80 L, designed pressure = 4 Mpa) through a plain orifice nozzle (diameter = 1.0 mm) directed vertically upward into test section at the room temperature and atmospheric pressure. The length-to-diameter ratio of the nozzle is 40, which enables the jet flow being fully developed. The inlet passage has a diameter of 4 mm and is followed by a convergent section before the straight injection orifice. Such configuration is designed to avoid cavitations during the experiment [18]. The nozzle is flush-mounted with the bottom of the test section. The large volume of the liquid storage tank provides a long enough time duration for liquid injection. The jet velocity v_j is measured by a pressure gauge. The cross airflow is supplied from a series of tanks (total volume 120 $\mathrm{m^3}$) arranged in such a way that the supply pressure remained nearly constant during tests (maximum working pressure 0.7 MPa). The crossflow first passes through a divergent section, and then into the rectifying chamber with a honeycomb inside. A uniform velocity profile is formed at the inlet of the test section after the air flowing through a contraction section. The uniform air flow velocity profile has been verified by experiment measurements. The test section (100 mm height× 40 mm width × 600 mm length) is made of plexiglass to provide optical access and clear view of the jet exit. The air velocity, u_G, is measured by a Pitot-static tube fitted at the centerline of the ceiling, 70 mm away from the inlet of test section, at the streamwise location of the nozzle. The measurement uncertainty of Pitot-static is less than ±5 Pa.

A high-speed camera is used to observe the round turbulent jet in uniform gaseous crossflows to investigate the bag and column breakup process. The illumination source employed in this study is a continuous light of 4500 lm. The images are recorded by a high-speed video camera (IDT X-Stream-3) with a maximum resolution of 1280 × 1024 pixels, maximum frame rate of 13,000 Hz, and minimum exposure time of 5 μs. The recording frequency varied from 2500 to 4100 Hz, and the exposure time varied from 15 to 20 μs depending on different test conditions.

B. Test Conditions

The test conditions are summarized in Table 1. The test liquid is the tap water. The subscript j denotes jet properties, L liquid properties, and G air properties. The Ohnesorge number was constant (<0.1) throughout the present study, thus the viscous effect can be neglected. The jet velocity varies from 4.6 to 8.1 m/s with an uncertainty less than 5%, and the air velocity varied from 25.2 to 46 m/s with an uncertainty less than 1%. The resulting ranges of liquid–air momentum ratio, q, and crossflow Weber number were 11–95 and 11–36, respectively.

III. Results and Discussion

A. Flow Visualization

The deformation of a liquid jet in crossflows is shown in Fig. 2. The air crossflow is obstructed by the presence of the liquid jet. As a result, the air flow velocity decreases quickly and the static pressure at the jet's upwind surface is increased. The enhanced differential static pressure between the upwind and downwind surfaces leads to the deformation of the jet. The cross section shape changes from circle to ellipse. As shown in Fig. 2, the diameter of the liquid jet decreases along the streamwise direction.

Continuously subjected to aerodynamic forces from the crossflow, the initially round shape liquid jet would deform as shown in the sketch of Fig. 3, and eventually develop into a bag. The gas pressure reduces along the side of the liquid jet as the crossflow is being accelerated over the liquid column. Therefore, the pressure inside the bag is greater than that outside. The pressure difference causes the membrane thickness and the ring diameter to decrease and increase, respectively. The deformation continues till the membrane is so thin that the surface tension is no longer enough to overcome the

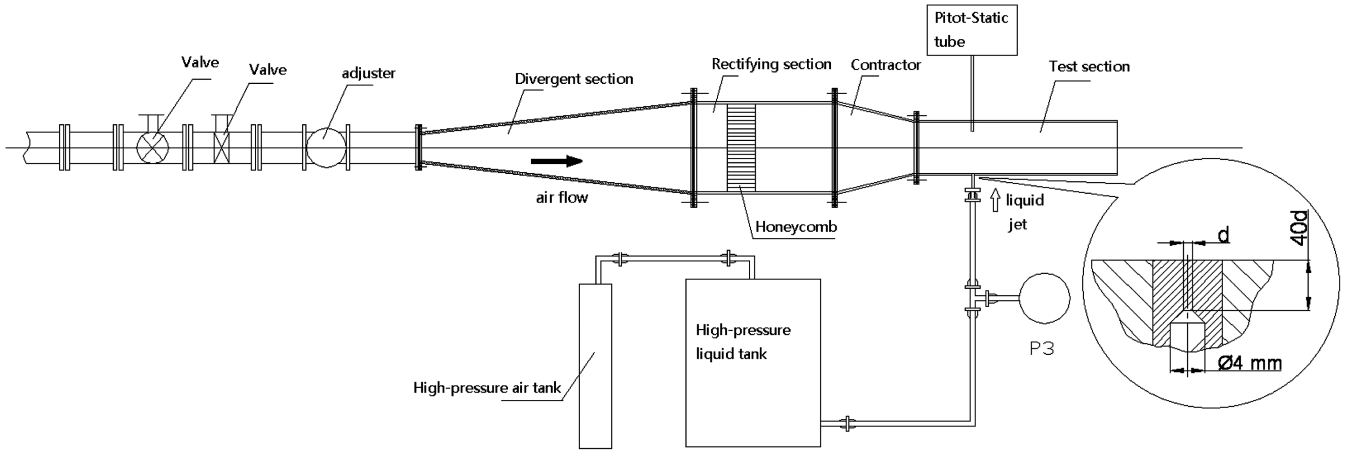

Fig. 1 Test apparatus.

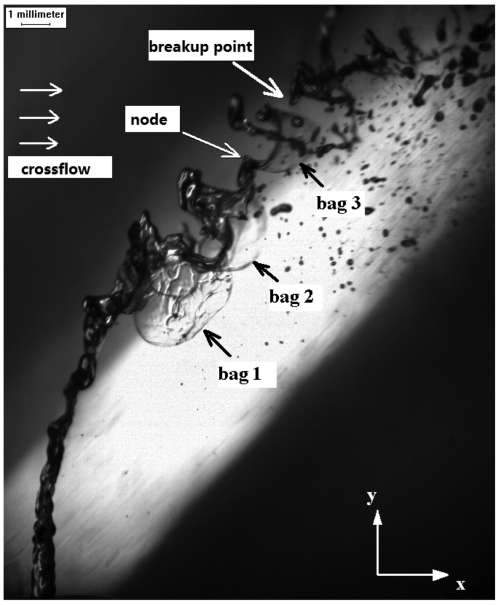

Fig. 2 A round liquid jet in uniform gaseous crossflows within the bag breakup regime ($d_0 = 1.0$ mm, $q = 26.22$, $We_G = 20$).

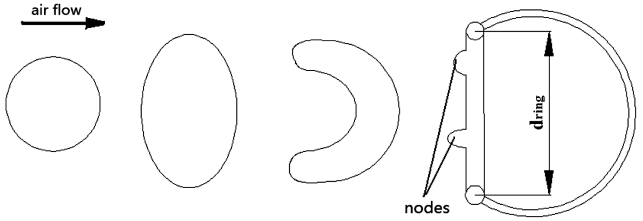

Fig. 3 The development of a liquid jet's cross section in uniform gaseous crossflows.

aerodynamic force. The membrane first breaks up into droplets. The remaining ring tube then falls into pieces in a Rayleigh-like breakup manner. At the end of the bag breakup process, three distinctive droplets are generated: 1) relatively large droplets associated with nodes called node-droplets; 2) ring-droplets due to the breakup of ring; and 3) a large amount of much smaller droplets generated by membrane breakup [14].

B. Force Balance on Bag

The Weber number is a crucial parameter to determine the breakup regime for a nonturbulent liquid jet in crossflows. By experimental observation, Mazallon et al. [10] proposed that for Oh number less than 0.1, the onset of the bag breakup initiates at a Weber number of 5. Theoretical analysis was conducted to predict the low Weber number boundary for bag breakup regime, and is presented in this paper.

For the analysis, it is assumed that the force balance is established when the diameter of the bag ring reaches a maximum value. The shape of the bag membrane is assumed to be a half-sphere with a diameter of d_r. A demonstration of the force balance is shown in Fig. 4.

Because of the presence of the bag, the air flow is quickly slowed down and almost all of the dynamic pressure is transferred into the static pressure. Therefore, the pressure inside the bag is larger than that outside. The force balance for a bag on the nonturbulent liquid jet can be written in a simplified form as follows:

$$(\text{differential static pressure})_{\text{bag}} = (\text{surface tension})_{\text{bag}} \tag{1}$$

$$\text{Or} \quad \frac{\pi d_r^2}{4} \times 1/2 \rho_G u_G^2 = \pi d_r \sigma \tag{2}$$

$$\text{Or} \quad \frac{\rho_G u_G^2 d_r}{\sigma} = 8 \tag{3}$$

In Eq. (3), d_r is unknown and can be provided by experiments.

C. Basal Ring Diameter

As discussed above, the basal ring diameter is required for the calculation of the Weber number at the beginning of the bag breakup. The measurements on the bag are shown in Fig. 5, where d_t denotes the diameter of bag ring tube which will be studied later.

The results of the basal ring diameter are shown in Fig. 6. The experiments show that the dimensionless diameter of the basal ring d_r/d_0 is almost a constant of about 2.85. This result is in good agreement with the parent drops being subjected to the secondary bag breakup during the transition between the stage of bag growth and bag breakup studied by Chou and Faeth [19]. It can be concluded that the basal ring diameter changes with neither jet nor crossflow velocity. Then the ratio between the surface breakup and the column breakup of a liquid column is largely decided by the number of bags along the jet, which has been studied be Ng et al. [15].

Substituting the equation $d_r/d_0 = 2.85$ into Eq. (3) gives

$$We_G = \frac{\rho_G u_G d_0}{\sigma} = \frac{\rho_G u_G d_r}{2.85\sigma} \approx 3 \tag{4}$$

There is some difference in the critical Weber number between our semi-empirical value of nearly 3 and the number reported by Mazallon et al. [10], which was 5. One of the possible reasons is that the present study used a turbulent liquid jet instead of a nonturbulent liquid jet, which was employed in Mazallon's study. More likely, the differential static pressure which is demanded to trigger the formation of a bag may be a little larger than that balances the surface

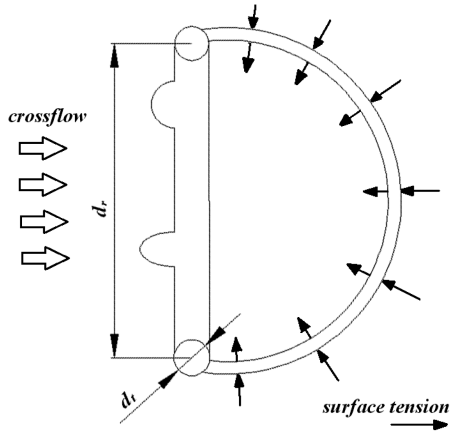

Fig. 4 Demonstration of the force balance for a bag.

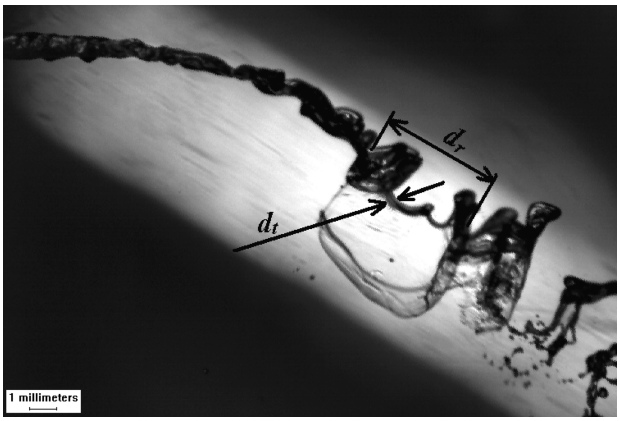

Fig. 5 Measurements on a bag.

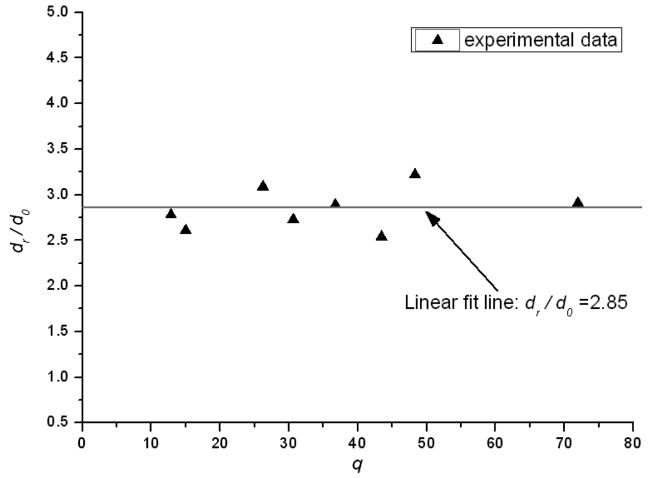

Fig. 6 Results of the basal ring diameter.

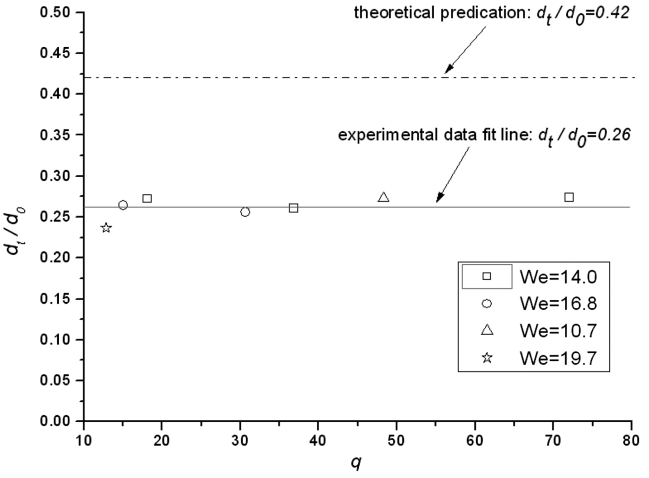

Fig. 8 Comparison of tube diameter between theoretical predication and experimental results.

tension. This is similar to the phenomenon that the starting current is larger than the working current or the starting friction is larger than the dynamic friction. In this case surface tension could not resist aerodynamic force during bag formation.

D. Diameter of Bag Ring Tube

Conservation of volume will apply to the process of the deformation of jet column. This can be used to determine the diameter of bag ring tube. Figure 7 has shown different sizes of a jet column and a bag. The bag is deformed from the jet column. l is the column height and d_0 is the initial jet diameter. While d_r is the basal ring diameter and d_t is the ring tube diameter mentioned above.

To simplify the analysis, nodes on the tube are not taken into consideration. Then according to the unchanged volume, one can write

$$C_1 \frac{\pi d_0^2}{4} l = \frac{\pi d_t^2}{4} \times \pi d_r \tag{5}$$

Here, C_1 is a proportion coefficient of the bag tube volume compared with the original jet column volume. Since $l \sim d_r$, Eq. (6) can be reduced into

$$C_1 \frac{\pi d_0^2}{4} d_r \approx \frac{\pi d_t^2}{4} \times \pi d_r \tag{6}$$

$$\text{Or} \quad d_t/d_0 = \sqrt{C_1/\pi} \tag{7}$$

However, the proportion coefficient C_1 was not determined in the primary breakup. Given the similarity between the primary and the secondary breakup, C_1 can be taken to be 0.56, similar to [19]. Substituting $C_1 \approx 0.56$ into Eq. (7), one can obtain

$$\frac{d_t}{d_0} = \sqrt{\frac{0.56}{\pi}} = 0.42 \tag{8}$$

According to Eq. (8), the dimensionless tube diameter d_t/d_0 is also a constant, which is not affected by the jet velocity and the crossflow velocity. The conclusion above has been justified by experiment results. However, the experimental and theoretical values are not the same. The theoretical analysis gives the value of 0.42, while the experimental fit provides a value of 0.26, as presented in Fig. 8.

The approximation of the column length l, as shown in Fig. 7 may have some effect on the uncertainty. Another significant reason could be the neglect of nodes. Apparently the volume of nodes, as shown in Fig. 5, is not negligible. Ignoring the nodes means their volume adds to the tube's volume. While the basal ring diameter remains unchanged, the enlarged volume makes the tube's diameter larger than its actual value.

Substituting $d_t/d_0 = 0.26$ into Eq. (7) yields $C_1 = 0.21$. This in turn means that nodes account for 35% of the initial volume. The volume of nodes is actually larger than that of the tube.

Since the bag membrane's volume is 44% of the initial volume, the volume conservation law can again be used as follows to obtain the membrane thickness:

$$1/2 \cdot 4\pi (d_r/2)^2 h = 0.44 \frac{\pi d_0^2}{4} l \tag{9}$$

$$\text{Or} \quad h = 0.22 (d_0/d_r)^2 d_r \tag{10}$$

$$\text{Or} \quad h = 0.22 d_0 \frac{d_0}{d_r} \tag{11}$$

where h is the membrane's thickness. Substituting $d_r/d_0 = 2.85$ into Eq. (11) yields

$$h = 0.08 d_0 \tag{12}$$

The membrane's thickness is very small compared with the initial jet diameter according to Eq. (12). Therefore, the droplets formed by the breakup of the membrane are certainly much smaller than others formed by the breakup of rings.

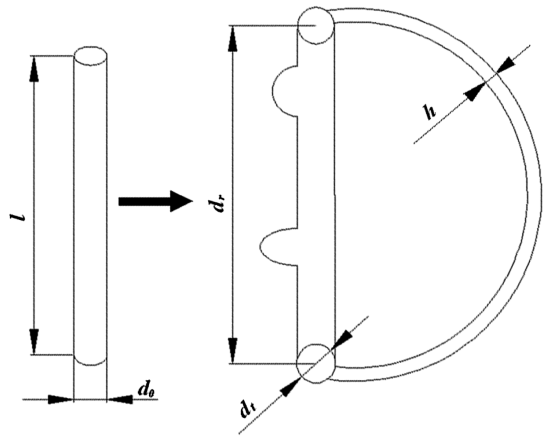

Fig. 7 Deformation from the jet column into a bag.

E. Bag Onset Length

As discussed above, the liquid column will undergo a distance of deformation before bags appear on the jet as shown in Fig. 9. Here

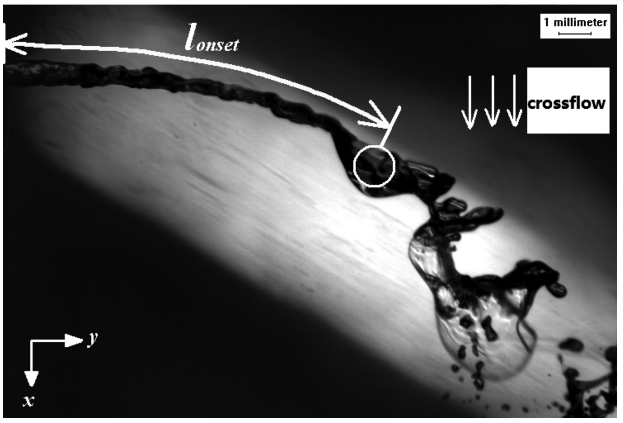

Fig. 9 The bag onset length of a liquid jet in uniform gaseous crossflows ($d_0 = 1.0$ mm, $q = 18$, $We_G = 14$).

this distance is defined as the bag onset length. The circle in Fig. 9 is a typical bag onset point.

The experimental observations of the bag onset length for various test conditions are plotted in Fig. 10 against the nondimensional number $\ell_n(q/Re_j)$. It is evident that the bag onset length l_{onset} is proportional to $\ell_n(q/Re_j)$. The length will extend longer when the momentum ratio is increased or the jet Reynolds number is reduced. The best fit correlation of the present measurements is given by

$$l_{\text{onset}}/d_0 = 8.33\,\ell_n(q/Re_j) + 56.7 \tag{13}$$

The correlation coefficient of the fit is 0.991. The term q/Re_j in Eq. (13) could be expressed as

$$q/Re_j = \frac{v_j \mu}{\rho_G u_G^2 d_0} \tag{14}$$

Since the bag onset length varies with the jet velocity and the square of the crossflow velocity, the influence of the air crossflow on the bag onset process is greater than that of the liquid jet. In other words, aerodynamics dominates the process.

According to [15], the streamwise velocity of the liquid column almost remains unchanged, nearly the same as the initial jet velocity. Thus the bag onset time t_{onset} equates to y_{onset}/v_j, where y_{onset} is the streamwise coordinate of the bag onset point. Unlike the onset length, the normalized bag onset time t_{onset}/t^* fluctuates around a constant of 1.9 as shown in Fig. 11, where t^* is the secondary characteristic breakup time proposed by Ranger and Nicholls [20], $t^* = d_0(\rho_j/\rho_G)^{1/2}/u_G$. Note that t^* only varies with the crossflow

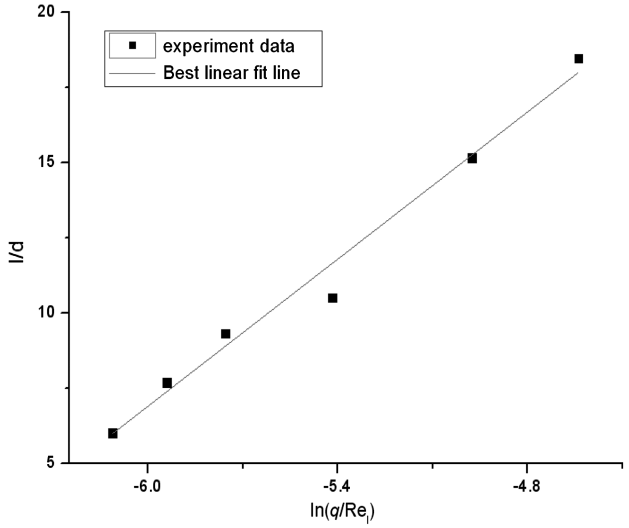

Fig. 10 Bag onset length as a function of dimensionless number $\ell_n(q/Re_j)$.

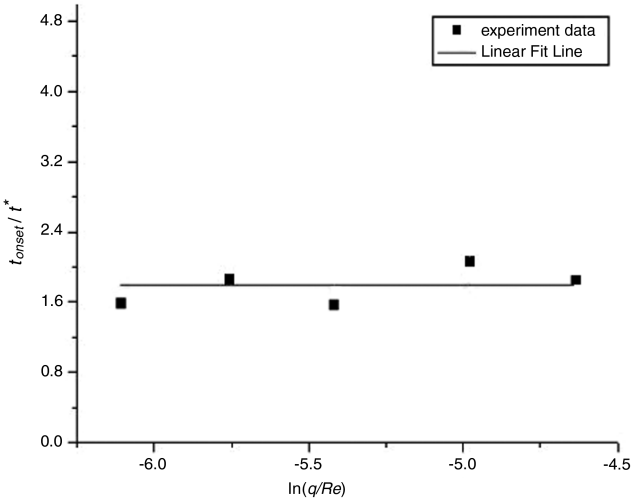

Fig. 11 Bag onset time as a function of dimensionless number $\ell_n(q/Rej)$.

velocity when referring to a certain gas, liquid, and injector. The bag onset time also correlates to the crossflow velocity alone.

Once the bag onset time is determined, the drag coefficient can be calculated as follows. A liquid column is considered, with the column experiencing a free-falling-like movement in crossflows. The aerodynamic force on the column is

$$F = C_D\left(\frac{1}{2}\rho_a u_a^2\right)(d_0 L) = \left(\rho_j \frac{\pi}{4} d_0^2 L\right)a \tag{15}$$

where C_D is the drag coefficient. Then the acceleration can be expressed as

$$a = \frac{2C_D \rho_a u_G^2}{\pi \rho_j d_0} \tag{16}$$

Then

$$t^* = d_0\left(\frac{\rho_j}{\rho_a u_G^2}\right)^{1/2} = \sqrt{\frac{2C_D}{\pi}}\sqrt{\frac{d_0}{a}} = C_2\sqrt{\frac{d_0}{a}} \tag{17}$$

$$\text{or} \quad d_0 = \frac{1}{C_2^2} a t^{*2} \tag{18}$$

Since the liquid column is subjecting to a movement like free-falling, the distance travelled after a period of t_{onset} from the initial position in the cross-stream direction can be given by

$$x_{\text{onset}} = 1/2 a t_{\text{onset}}^2 \tag{19}$$

Dividing Eq. (19) by Eq. (18), one can obtain

$$t_{\text{onset}}/t^* = \sqrt{2C_3/C_2^2} \tag{20}$$

where $C_3 = x_{\text{onset}}/d_0$, and equates to 2.75 according to experiments. Substituting $t_{\text{onset}}/t^* = 1.9$ in Eq. (20) yields

$$2C_3/C_2^2 = \frac{2 \times 2.75}{2C_D/\pi} = \frac{2.75\pi}{C_D} = 1.9^2 \tag{21}$$

Then the drag coefficient is found to be $C_D = 2.4$. Such drag coefficient is about 2.8 times larger than that for a cylinder in the same test condition. This is simply due to the increasing projection area of the liquid jet in crossflows after the deformation.

Generally, the momentum ratio is assumed to be the only parameter that determines the trajectory of the liquid jet in crossflows. As the bag onset point is surely on the liquid jet, it should vary with the momentum ratio exclusively. The best fit correlations of the present measurements are given by

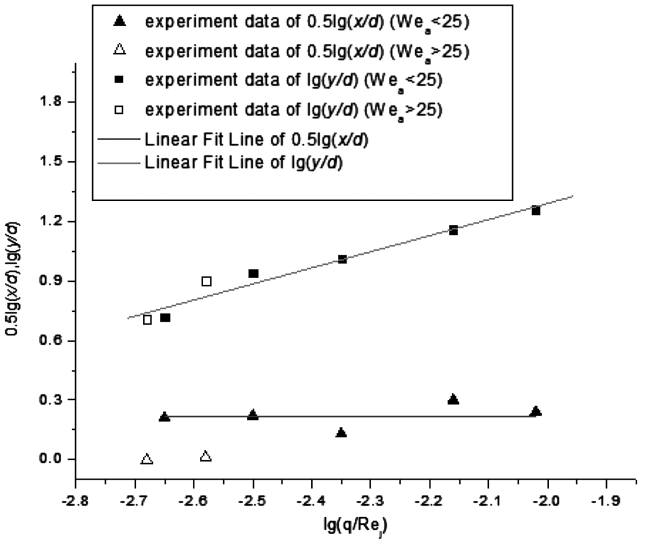

Fig. 12 Bag onset point as a function of dimensionless number $\ell_n(q/Re_j)$.

$$y_{\text{onset}}/d_0 = 1.395q^{0.57} \quad We_G < 25 \tag{22}$$

$$x_{\text{onset}}/d_0 = 2.75 \quad We_G < 25 \tag{23}$$

The correlation coefficients of the fits are 0.934 and 0.90, respectively. Yet further research shows that y_{onset}/d_0 correlates better with q/Re_j than with q as shown in Fig. 12, and the best fit correlation is given by

$$y_{\text{onset}}/d_0 = 10^{2.9}(q/Re_j)^{0.8} \tag{24}$$

The hollow symbols in Fig. 12 are the cases that the crossflow Weber number is greater than 25. The left hollow symbols indicate the case of the crossflow Weber number of 36, and the right hollow symbols indicate the case of the crossflow Weber number of 28.4. If the crossflow Weber number is greater than 25, the y direction coordinates still agree with Eq. (22) as shown in Fig. 12. Yet the corresponding x direction coordinates decrease, and x_{onset}/d_0 becomes about 1.0. The way of the bag onset near the transition into multimode breakup regimes is different from that of the bag breakup regime. The breakup phenomenon near the transition starts to present some similarities of the multimode breakup regime.

F. Bag Breakup Distance

The deformation of the jet cross section from a circle to an ellipse is driven by aerodynamics, which further results into the bag formation. After a certain distance, the bag membrane would break up when surface tension is no longer able to overcome the aerodynamic force, as shown in Fig. 13. Here the curve length between the bag onset point and the breakup point is defined as the bag breakup distance.

The time duration corresponding to the bag breakup distance is found to be a constant in this study, $t_{\text{bag}}/t^* = 1.58$, which is much smaller than the characteristic bag breakup time of the secondary breakup, $t_{\text{bag}}/t^* = 4$ [21]. While the breakup time stays as a constant, the bag breakup distance varies with different crossflow Weber numbers as shown in Fig. 14. The influence of the jet velocities, which have small values, on the bag breakup distance can be neglected. However, further investigations about the jet velocity influence need to be done.

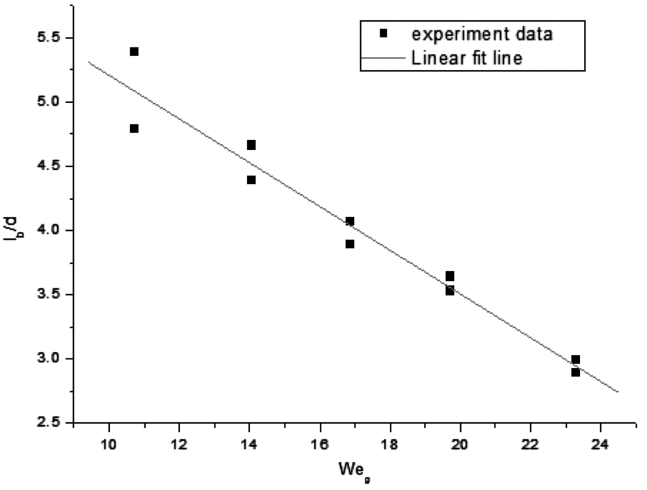

Fig. 14 Bag breakup distance as a function of the crossflow Weber Number.

A best fit from Fig. 14 is obtained as follows for the present range of the test conditions, $11 < We_G < 23$:

$$l_{\text{bag}}/d = 6.91 - 0.17We_G \tag{25}$$

A larger Weber number would reduce the bag breakup distance and lead to a better atomization. Also as observed in Fig. 14, the scattering of data points tends to diminish as the crossflow Weber number increases. Therefore, both the jet velocity and the crossflow velocity influence the bag breakup distance when they are at the same order of magnitude. On the contrary, crossflows dominate the bag breakup process, for example in the case of $\Delta v > 26$ m/s.

G. Jet Breakup Location

Another type of breakup is the column breakup. The core jet breakup destroys the continuity of the jet. As shown in Fig. 2, a liquid column breaks up into discontinued droplets after the jet breakup location. The droplet breakup is a secondary breakup which is not taken into consideration in this study. So it is crucial to investigate the location of the jet breakup point. The time-averaged jet breakup points are obtained corresponding to different test conditions and these points' coordinates are correlated to the liquid–air momentum flux ratio q, as shown in Fig. 15.

The normalized streamwise coordinate of the jet breakup point $\ell_n(y_b/d_0)$ varies proportionally with the momentum ration $\ell_n(q)$. Unlike the conclusion of the column breakup regime [11], the cross-stream coordinate almost remains unchanged, $x_b/d_0 = 7.9$. Neither the jet nor the crossflow velocity affects the cross-stream location of the jet breakup point. This conclusion agrees well with Wu et al.'s [4] observation of $x_b/d_0 = 8.06$. The discrepancy between the values of the present and their studies can be attributed to experimental uncertainty. The best fit correlation of the present measurements of

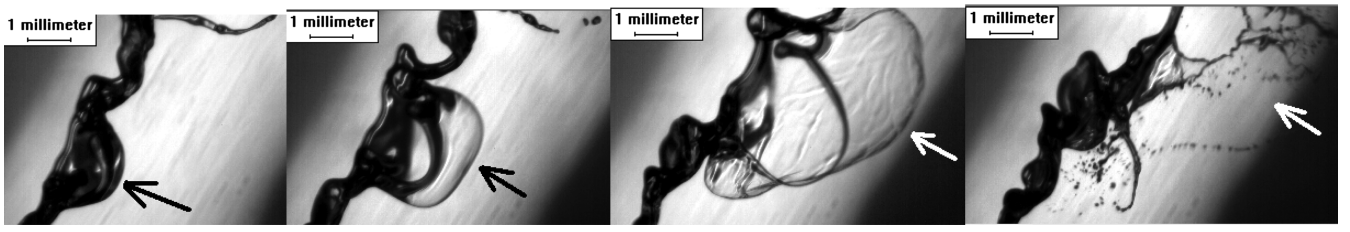

Fig. 13 Bag breakup process ($q = 36.7$, $We_G = 14$, $Re_j = 7000$).

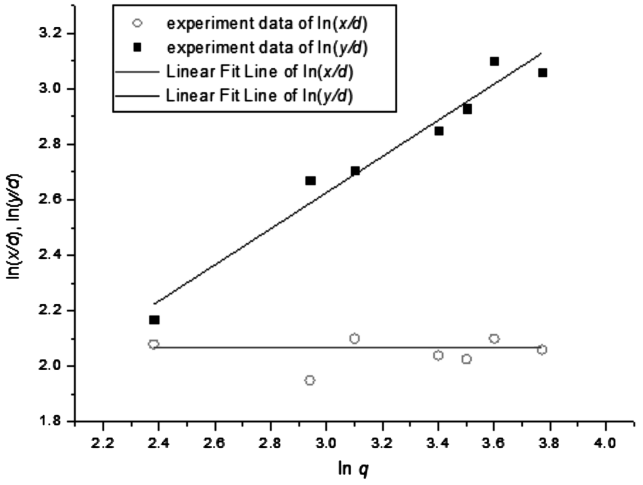

Fig. 15 Liquid jet breakup location as a function of dimensionless number $\ell_n q$.

the streamwise location of the jet breakup location in the bag breakup regime is given by

$$y_b/d_0 = 1.975q^{0.62} \tag{26}$$

The correlation coefficient of the fit is 0.95. Combined with the definition of the momentum ratio q, one can see that increasing the jet velocity or decreasing the crossflow velocity would delay the onset of the core jet breakup.

IV. Conclusions

An experimental study was conducted on the bag breakup regime of a liquid jet in gaseous crossflows. A high-speed camera was employed to investigate the bag size (including the ring diameter and the tube diameter), the bag onset length, and the jet breakup location. Test conditions were limited to water jet through a pressure-fed plain orifice nozzle of 1.0 mm, with the crossflow Weber number 11–28, liquid–air momentum flux ratio 11–95, and small Oh numbers (<0.1). The main conclusions are as follows:

1) An analysis of the force balance on bags is conducted and a criterion for the bag formation is obtained. The diameter of the basal ring tube is predicted according to a reduced-order model.

2) The normalized bag ring diameter and ring tube diameter remain constants at different test conditions.

3) The normalized bag onset length l_{onset}/d is proportional to $\ell_n(q/Re_j)$. Either increasing the liquid–air momentum flux ratio or reducing the jet Reynolds number would elongate the bag onset length. In contrast, the bag onset time is independent of test conditions.

4) The jet velocity has no significant effect on the bag breakup length, while increasing the air velocity or the crossflow Weber number would decrease the length.

5) The jet breakup location only correlates with the liquid–air momentum flux ratio. Specifically, the normalized cross-stream location of the jet breakup point is independent of the momentum ratio and stays as a constant of $7.9d_0$. The streamwise coordinate of the jet breakup location increases linearly with $q^{0.62}d_0$.

Acknowledgments

This paper was financially supported by Chinese 111 Project, Grant No. B08009. The authors appreciate the assistance with English writing from Joseph J. Wang from University of Southern California and S. B. Tambe from University of Cincinnati.

References

[1] Lefebvre, A. H., *Atomization and Sprays*, Hemisphere Publishing Corp., New York, 1989, Chap. 4.

[2] Cavaliere, A., Ragucci, R., and Noviello, C., "Bending and Break-up of a Liquid Jet in a High Pressure Airflow," *Experimental Thermal and Fluid Science*, Vol. 27, No. , 2003, pp. 449–454.

[3] Aalburg, C., Sallam, K. A., and Faeth, G. M., "Properties of Nonturbulent Round Liquid Jets in Uniform Crossflows," *42nd AIAA Aerospace Sciences Meeting and Exhibit*, AIAA, Reston, VA, 2004.

[4] Wu, P. K., Kirkendall, K. A., Fuller, R. P., and Nejad, A. S., "Breakup Processes of Liquid Jets in Subsonic Crossflows," *Journal of Propulsion and Power*, Vol. 13, No. 1, 1997, pp. 64–73.

[5] Sallam, K. A., Aalburg, C., and Faeth, G. M., "Breakup of Round Nonturbulent Liquid Jets in Gaseous Crossflows," *41st AIAA Aerospace Sciences Meeting and Exhibit*, AIAA, Reston, VA, 2003.

[6] Tambe, S. B., Jeng, S. M., Mongia, H., and Hsiao, G., "Liquid Jets in Subsonic Crossflow," *43rd AIAA Aerospace Sciences Meeting and Exhibit*, AIAA, Reston, VA, 2005.

[7] Wu, P. K., Kirkendall, K. A., and Fullern, R. P., "Spray Structures of Liquid Fuel Jets Atomized in Subsonic Crossflows," *Journal of Propulsion and Power*, Vol. 14, No. 2, 1998, pp. 173–182. doi:10.2514/2.5283

[8] Becker, J., and Hassa, C., "Breakup and Atomization of Kerosene Jet in Crossflow at Elevated Pressure," *Atomization and Sprays*, Vol. 12, Nos. 1–3, 2002, pp. 49–67. doi:10.1615/AtomizSpr.v12.i123.30

[9] Lin, K.-C., Kennedy, P. J., and Jackson, T. A., "Penetration Heights of Liquid Jets in High-Speed Crossflows," *40th AIAA Aerospace Sciences Meeting and Exhibit*, AIAA, Reston, VA, 2002.

[10] Mazallon, J., Dai, Z., and Faeth, G. M., "Aerodynamic Primary Breakup at the Surface of Nonturbulent Round Liquid Jets in Crossflow," *36th Aerospace Sciences Meeting and Exhibit*, AIAA, Reston, VA, 1998.

[11] Zhu, Y., Huang, Y., Wang, F., and Wang, X. H., "Experiment on Breakup Processes and Surface Waves of Round Liquid Jets in Crossflows," *Proceedings of ASME Turbo Expo 2010*, ASME, Fairfield, NJ, 2010.

[12] Zhu, Y., Huang, Y., Wang, F., and Wang, X. H., "Experiment on Breakup Processes of Round Liquid Jets in Crossflows," *Journal of Aerospace Power*, Vol. 25, No. , 2010, pp. 2261–2266 (in Chinese).

[13] Aalburg, C., Faeth, G. M., and Sallam, K. A., "Primary Breakup of Round Turbulent Liquid Jets in Uniform Crossflows," *43rd AIAA Aerospace Sciences Meeting and Exhibit*, AIAA, Reston, VA, 2005.

[14] Sallam, K. A., Ng, C.-L., Sankarakrishnan, R., Aalburg, C., and Lee, K., "Breakup of Turbulent and Nonturbulent Liquid Jets in Gaseous Crossflows," *44th AIAA Aerospace Sciences Meeting and Exhibit*, AIAA, Reston, VA, 2006.

[15] Ng, C.-L., Sankarakrishinan, R., and Sallam, K. A., "Bag Breakup of Nonturbulent Liquid Jets in Crossflow," *International Journal of Multiphase Flow*, Vol. 34, No. 3, 2008, pp. 241–259. doi:10.1016/j.ijmultiphaseflow.2007.07.005

[16] Zhu, Y., Huang, Y., and Guo, Z., "Experiment on Round Liquid Jet Deformation and Breakup Length," *Symposium of Ramjet Engine Technology*, Jilin, 2005 (in Chinese).

[17] Wan, Y., Huang, Y, and Zhu, Y., "Experiment on the Breakup Process of Free Round Liquid Jet," *Journal of Aerospace Power*, Vol. 23, No. 2, 2008, pp. 208–214 (in Chinese).

[18] Reitz, R. D., and Bracco, F. V., "Mechanism of Atomization of a Liquid Jet," *Physics of Fluids*, Vol. 25, No. 10, 1982, pp. 1730–1742. doi:10.1063/1.863650

[19] Chou W.-H., and Faeth, G. M., "Temporal Properties of Secondary Drop Breakup in the Bag Breakup Regime," *International Journal of Multiphase Flow*, Vol. 24, No. 6, 1998, pp. 889–912. doi:10.1016/S0301-9322(98)00015-9

[20] Ranger, A. A., and Nicholls, J. A., "The Aerodynamic Shattering of Liquid Drops," *AIAA Journal*, Vol. 7, No. 2, 1969, pp. 285–290. doi:10.2514/3.5087

[21] Chou W.-H., Hsiang L.-P., and Faeth, G. M., "Dynamics of Drop Deformation and Formation During Secondary Breakup in the Bag Breakup Regime," AIAA Paper No. 1997-0797, 1997.

R. Lucht
Associate Editor